NMR Studies of the E140Q Mutant of the Carboxy-Terminal Domain of Calmodulin Reveal Global Conformational Exchange in the Ca^{2+}-Saturated State†

Johan Evenäs,* Eva Thulin, Anders Malmendal, Sture Forsén, and Göran Carlström

Physical Chemistry 2, Center for Chemistry and Chemical Engineering, Lund University, P.O. Box 124, S-22100 Lund, Sweden

Received November 15, 1996; Revised Manuscript Received January 16, 1997⊗

ABSTRACT: In the present investigation, the Ca^{2+} activation of the C-terminal domain of bovine calmodulin and the effects of replacing the bidentate Ca^{2+}-coordinating glutamic acid residue in the 12th and last position of loop IV with a glutamine are studied by NMR spectroscopy. The mutation E140Q results in sequential Ca^{2+} binding in this domain and has far-reaching effects on the structure of $(Ca^{2+})_2$ TR_2C, thereby providing further evidence for the critical role of this glutamic acid residue for the Ca^{2+}-induced conformational change of regulatory EF-hand proteins. Analyses of the NOESY spectra of the mutant under Ca^{2+}-saturated conditions, such that 97% of the protein is in the $(Ca^{2+})_2$ form, revealed two sets of mutually exclusive NOEs. One set of NOEs is found to be consistent with the closed structure observed in the apo state of the C-terminal domain of the wild-type protein, while the other set supports the open structure observed in the Ca^{2+}-saturated state. In addition, several residues in the hydrophobic core exhibit broadened resonances. We conclude that the $(Ca^{2+})_2$ form of the mutant experiences a global conformational exchange between states similar to the closed and open conformations of the C-terminal domain of wild-type calmodulin. A population of 65 ± 15% of the open conformation and an exchange rate of $(1-7) \times 10^4$ s^{-1} were estimated from the NMR data and the chemical shifts of the wild-type protein. From a Ca^{2+} titration of the ^{15}N-labeled mutant, the macroscopic binding constants [$\log(K_1) = 4.9 \pm 0.3$ and $\log(K_2) = 3.15 \pm 0.10$] and the inherent chemical shifts of the intermediate $(Ca^{2+})_1$ form of the mutant were determined using NMR. Valuable information was also provided on the mechanism of the Ca^{2+} activation and the roles of the structural elements in the two Ca^{2+}-binding events. Comparison with the wild-type protein indicates that the $(Ca^{2+})_1$ conformation of the mutant is essentially closed but that some rearrangement of the empty loop IV toward the Ca^{2+}-bound form has occurred.

Calmodulin (CaM)[1] is a ubiquitous intracellular eukaryotic protein, activated by binding of calcium ions. In the Ca^{2+}-saturated form, it binds and regulates more than 25 different target proteins involved in a variety of different cell functions (Klee, 1988; Crivici & Ikura, 1995; Finn & Forsén, 1995). The protein consists of 148 amino acids and is highly conserved among different eukaryotic species. CaM belongs to the superfamily of proteins containing EF hands, Ca^{2+}-binding helix−loop−helix structural motifs (Kretsinger & Nockolds, 1973), which generally appear in pairs and often show cooperative binding of calcium. The homologous EF-hand proteins are, broadly speaking, involved in two important functionalities: Ca^{2+} buffering or transport and Ca^{2+}-dependent regulation of cell functions. Calcium binding to the regulatory EF-hand proteins causes substantial structural changes, as demonstrated by the three-dimensional (3D) structures obtained by X-ray crystallography and NMR spectroscopy of CaM (Babu et al., 1988; Chattopadhyaya et al., 1992; Kuboniwa et al., 1995; Zhang et al., 1995) and troponin C (TnC) (Herzberg & James, 1988; Gagné et al., 1995), which initiate further cellular responses. On the other hand, Ca^{2+} binding to the Ca^{2+}-buffering proteins does not induce major conformational changes, as indicated, for example, by the structures of calbindin D_{9k} (Szebenyi & Moffat, 1986; Kördel et al., 1993; Skelton et al., 1994).

CaM consists of four EF-hand repeats. The N- and C-terminal EF-hand pairs form two distinct domains separated by a tether region. The two domains are structurally similar and have the two EF hands packed in a roughly parallel fashion with a short β-sheet interaction between the Ca^{2+}-binding loops (Figure 1). The helices are denoted A−H and the four binding loops I−IV. Within each domain, the two EF hands are connected by a short linker between helices B and C and between helices F and G, respectively. Upon Ca^{2+} binding to CaM, the secondary structural elements in both domains remain essentially unchanged while their relative orientations change from a closed to an open structure. In the C-terminal domain, for example, helices E and H become more perpendicular to helices F and G. These reorientations are associated with the repositioning of many side chains and result in the exposure of well-defined hydrophobic patches in both domains where target molecules may be bound. The tether between the two domains was initially seen as a long central helix in crystal structures but was later shown by NMR spectroscopy to be mobile in solution (Barbato et al., 1992). This flexibility permits the

† This research was supported by grants from the Swedish Natural Science Research Council and the EU COST program. The 600 MHz NMR spectrometer was purchased by a grant from the Knut and Alice Wallenberg Foundation.

* Author to whom correspondence should be addressed.

⊗ Abstract published in *Advance ACS Abstracts,* March 1, 1997.

[1] Abbreviations: 3D, three dimensional; COSY, correlation spectroscopy; CaM, calmodulin; E140Q, E140Q mutant of the carboxy-terminal tryptic fragment of calmodulin (M76−K148); HSQC, heteronuclear single-quantum coherence spectroscopy; NMR, nuclear magnetic resonance; NOE, nuclear Overhauser effect; NOESY, nuclear Overhauser effect spectroscopy; TnC, troponin C; TOCSY, total correlation spectroscopy; TR_2C, carboxy-terminal tryptic fragment of calmodulin (M76−K148); wt, wild type.

S0006-2960(96)02827-9 CCC: $14.00

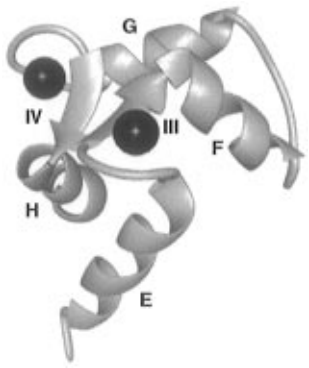

FIGURE 1: Ribbon representation of Ca^{2+}-saturated TR_2C, the carboxy-terminal domain of calmodulin (Babu et al., 1988). The helices are indicated with E, F, G, and H and the Ca^{2+}-binding loops with III and IV. The figure was generated using UCSF software MidasPlus (Ferrin et al., 1988).

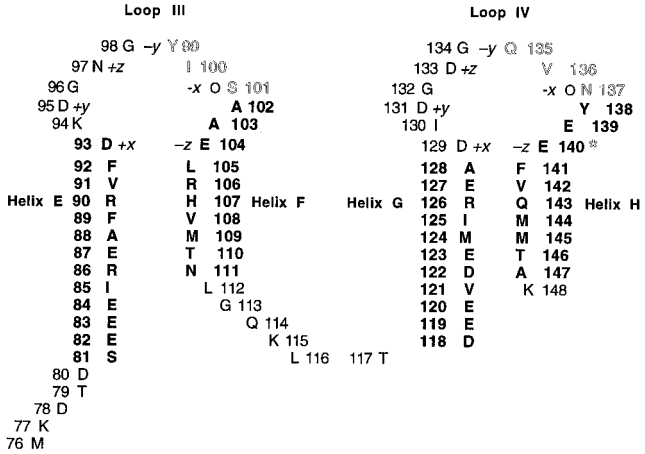

FIGURE 2: Amino acid sequence of TR_2C, the carboxy-terminal tryptic fragment of bovine calmodulin, expressed in *E. coli*. The Ca^{2+} ligands are denoted by the approximate Cartesian coordination: $+x$, $-z$, etc. The residue in position 9 (○) in each loop coordinates the calcium ion via a water molecule. Helical residues are denoted in bold letters and residues in β-strands are outlined. The mutated residue is indicated by an open star.

domains to bend toward each other and cooperate in binding of target molecules. The consensus sequence for the Ca^{2+}-binding loop is 12 residues long, and position 1 is found near the C-terminus of the preceding helix. After a conserved glycine in position 6, residues in positions 7−9 take part in the β-strand interacting with the neighboring binding loop. The last three loop residues are located in the N-terminus of the trailing helix. The geometry of the Ca^{2+} coordination can be described as a pentagonal bipyramide where five of the seven Ca^{2+} ligands are provided by side chain carboxylate oxygens from residues in positions 1, 3, 5, and 12 (a bidentate ligand). The two remaining Ca^{2+} ligands are provided by the backbone carbonyl oxygen of residue 7 and a water molecule.

In intact CaM, each domain exhibits cooperative binding of two calcium ions, with dissociation constants in the micromolar range. Similar Ca^{2+}-binding characteristics are reported (Linse et al., 1991) for the two tryptic fragments of bovine CaM corresponding to each domain, TR_1C (residues 1−77) and TR_2C (residues 78−148) (Drabikowski et al., 1977; Walsh et al., 1977). Furthermore, structural autonomy of the individual domains is indicated by the reported 3D structures of apo and $(Ca^{2+})_2$ TR_2C (Finn et al., 1995). This domain independence suggests that the individual domains, TR_1C and TR_2C, are useful and relevant models of CaM in studies of the structural and dynamical responses upon Ca^{2+} binding.

The molecular mechanism for cooperativity between paired EF hands in Ca^{2+} binding is not yet fully understood. Suggestions of loop−loop interactions mediated by the β-sheet and by structural rearrangements of the hydrophobic core have been made for calbindin D_{9k} and CaM (Wimberly et al., 1995; George et al., 1996). For a detailed understanding of the cooperativity, it is important to also characterize the protein at intermediate calcium levels. Studies of calbindin D_{9k} have indicated that changes in both protein structure and dynamics upon binding of the first ion significantly contribute to the cooperativity (Akke et al., 1991; Wimberly et al., 1995). Studies of the $(Ca^{2+})_1$ state are not possible for wild-type TR_2C (wt-TR_2C), as the strong cooperativity prevents the observation of this intermediate form in solution. We have attempted to circumvent this difficulty and gain more insight into the mechanism of Ca^{2+} activation of CaM by studying TR_2C in the apo, $(Ca^{2+})_1$, and $(Ca^{2+})_2$ forms using site-directed mutagenesis to decrease the binding affinity of one of the loops. We have chosen to study a mutant where the glutamic acid residue in the 12th position of loop IV of bovine TR_2C is mutated to a glutamine (E140Q). Two Ca^{2+} ligands are provided by the side chain of this conserved residue, coordinating the ion with both carboxylate oxygens. The amino acid sequence with the Ca^{2+} coordination and secondary structure of bovine TR_2C is shown in Figure 2.

In earlier studies of CaM and other EF-hand proteins (Beckingham, 1991; Maune et al., 1992b; Carlström & Chazin, 1993; Shea et al., 1996), the role of the glutamic acid residue in the 12th position of Ca^{2+}-binding loops has been explored. In regulatory EF-hand proteins, this glutamic acid residue is generally believed to be important for the conformational changes to occur upon Ca^{2+} binding. In studies of mutants where the glutamic acid residue has been mutated to a glutamine, sizable effects on the protein have been observed. The Ca^{2+} affinity is decreased by a factor of approximately 10^4 for the mutated site in *Drosophila* CaM (Maune et al., 1992b) as well as in calbindin D_{9k} (Carlström & Chazin, 1993). The observed changes in chemical shift in the NMR spectra upon Ca^{2+} binding to the E140Q mutant of *Drosophila* CaM occurred in the fast-exchange regime on the NMR time scale (Starovasnik et al., 1992), in contrast to the behavior of wt-TR_2C, which exhibits slow exchange (Thulin et al., 1984). The fast-exchange behavior of the mutant has been shown to be the consequence of an increase in the off-rate (Martin et al., 1992).

In the present study we have made ^1H and ^{15}N assignments of NMR spectra of the apo and $(Ca^{2+})_2$ forms of E140Q and also investigated the NOEs and made comparisons to wt-TR_2C. A Ca^{2+} titration to E140Q monitored by 2D ^{15}N HSQC spectra provided the macroscopic Ca^{2+}-binding constants and indirectly the backbone ^1H and ^{15}N assignments of the $(Ca^{2+})_1$ form of E140Q as well as information about the molecular mechanisms of the Ca^{2+}-binding processes.

EXPERIMENTAL PROCEDURES

Synthesis of the E140Q Mutant of TR_2C and Protein Production. The synthetic gene of the TR_2C domain of

bovine CaM was constructed from overlapping oligonucleotides (Brodin, unpublished) essentially as described for bovine calbindin D_{9k} (Brodin et al., 1986). The mutation was made with the mismatch method using the kit Muta-Gene M13 *In Vitro* Mutagenesis from Bio-Rad. The gene for E140Q was completely cloned into the plasmid pRCB1. Expression and purification of unlabeled and ^{15}N-labeled E140Q were carried out using an expression system previously employed for the production of wt-TR_2C (Finn et al., 1995).

NMR Sample Preparation. For all NMR samples, purified apo E140Q was dissolved to concentrations of 1−3 mM in H_2O with 10% D_2O and 100 μM NaN_3. Aliquots of calcium were added to the samples as solutions of $CaCl_2 \cdot 2H_2O$. All experiments were performed at 28 °C and pH 6.0.

NMR Spectroscopy, Data Processing, and Analysis. For all homonuclear NMR experiments, water suppression was accomplished by a weak presaturation of 1.3 s. A General Electric Omega 500 spectrometer operating at 500.13 MHz for protons was used for acquisition of 2D ^{1}H COSY (Aue et al., 1976) and 2D ^{1}H NOESY (Macura & Ernst, 1980; Bax, 1985) spectra, with a NOESY mixing time of 200 ms. All other experiments were run on a Varian Unity Plus spectrometer at 599.89 MHz for protons. A sensitivity-enhanced 2D ^{15}N HSQC with gradient selection and a water-flip-back pulse (Zhang et al., 1994) was used for the titration series. The spectra were recorded with 64 and 640 complex data points in t_1 and t_2, respectively, and a relaxation delay of 1.5 s. The spectral widths were 1650 and 8000 Hz in the ^{15}N dimension and the ^{1}H dimension, respectively. Using two scans per t_1 increment, the total experimental time was 8 min per spectrum. The ^{15}N nuclei were decoupled during acquisition using the WALTZ-16 sequence (Shaka et al., 1983). To check and facilitate the assignments, we recorded a homonuclear 2D ^{1}H NOESY, a 2D ^{15}N HSQC-TOCSY with a DIPSI-2 relaxation compensated isotropic mixing sequence (Cavanagh & Rance, 1992), and a 3D ^{15}N NOESY-HSQC spectrum (Zhang et al., 1994) of E140Q at 21 equiv of calcium. The NOESY mixing time was 200 ms in both cases, and the TOCSY mixing time was 100 ms. All spectra were processed and analyzed using Felix95 (BIOSYM Technologies, San Diego).

NMR Assignments. ^{1}H chemical shifts are referenced to the ^1H_2O signal at 4.725 ppm at 301 K (Hartel et al., 1982; Orbons et al., 1987). Indirect referencing is used for the ^{15}N chemical shifts using the frequency ratio (^{15}N/^{1}H) of 0.101329118 where the ^{1}H frequency is that of DSS in water (Wishart et al., 1995). ^{1}H NMR assignments of backbone protons in apo E140Q were obtained using the homonuclear COSY and NOESY spectra recorded in H_2O. The assignment procedure was straightforward, following the amide-proton-based strategy (Chazin & Wright, 1987) and facilitated by the close resemblance to the assignments of apo wt-TR_2C reported by Finn et al. (1993). The ^{15}N HSQC spectrum was then assigned on the basis of these assignments and the ^{15}N shifts of apo wt-TR_2C (Bryan E. Finn, personal communication). By following the cross-peaks in the ^{15}N HSQC titration series, the amide nitrogens and protons of $(Ca^{2+})_2$ E140Q were preliminary assigned. They were then subsequently checked, and in a few cases corrected, by assigning all nonlabile protons and amide nitrogens using the ^{1}H NOESY, 2D ^{15}N HSQC-TOCSY, and 3D ^{15}N NOESY-HSQC spectra.

NMR Titration. 2D ^{15}N HSQC spectra were recorded for E140Q at 14 different Ca^{2+} concentrations. The final protein and Ca^{2+} concentrations were determined by amino acid hydrolysis and atomic absorption spectrophotometry, respectively, and corresponded to 21 equiv of calcium relative to the protein. In order to be able to observe the weak cross-peaks of Y138 and F141, broadened beyond detection at the highest Ca^{2+} concentration, an additional ^{15}N HSQC-spectrum with 96 scans was recorded.

Determination of Binding Constants. The apo shifts, δ_{apo}, were taken directly from the ^{15}N HSQC spectrum of the apo state. The two macroscopic binding constants, K_1 and K_2, and the chemical shifts of the $(Ca^{2+})_1$ and $(Ca^{2+})_2$ forms for each nuclei, δ_{Ca1} and δ_{Ca2}, were determined by simultaneous fitting to the observed chemical shifts of 25 arbitrarily chosen amide nuclei at 15 different Ca^{2+} concentrations. In total 52 variables were determined by minimizing the function

$$\sum_{i}^{15}\sum_{j}^{25}[(1 - p_{Ca1}(i) - p_{Ca2}(i))\delta_{apo}(j) + p_{Ca1}(i)\delta_{Ca1}(j) + p_{Ca2}(i)\delta_{Ca2}(j) - \delta_{obs}(i,j)]^2 \quad (1)$$

where $p_{Ca1}(i)$ and $p_{Ca2}(i)$ are the relative populations of the $(Ca^{2+})_1$ and the $(Ca^{2+})_2$ state, respectively, calculated from the binding constants and the protein concentration at Ca^{2+} concentration i and $\delta_{obs}(i,j)$ is the observed chemical shift for nucleus j at Ca^{2+} concentration i.

The minimization problem was solved using a simulated annealing algorithm. Initial values of δ_{Ca1} and δ_{Ca2} were estimated from the binding curves. The algorithm used a 52-dimensional box centered around these values with the side lengths corresponding to the estimated error limits. Within this box 10 000 sets of random variables were created. The set with the lowest residual was then chosen as the center of a new smaller box. The procedure was repeated until the error in the optimized values was considered below the experimental errors. The errors in the optimization were estimated from repeating the whole algorithm several times. Since the Ca^{2+}-binding constant of the mutated loop IV is approximately 2 orders of magnitude lower than for loop III, only the $(Ca^{2+})_1$ state with a calcium ion bound to loop III was considered.[2] Effects from increased ionic strength during the titration were neglected.

RESULTS AND DISCUSSION

A first step to verify that a mutant is a suitable model for the wild-type protein is to compare the proteins in the apo and Ca^{2+}-saturated states. Complete backbone and side chain ^{1}H and ^{15}N assignments of apo and $(Ca^{2+})_2$ E140Q were obtained from the NMR spectra. The chemical shifts of backbone amide nuclei of the $(Ca^{2+})_1$ form were calculated from the NMR data of the Ca^{2+} titration as described in detail below. The chemical shifts of ^{15}N and NH backbone nuclei of all three states are given as Supporting Information.

Apo E140Q. Figure 3 shows the chemical shift differences of the backbone amide protons between the apo states of E140Q and wt-TR_2C (filled bars). The comparison reveals

[2] Since sequential binding is obtained in E140Q, the observed macroscopic binding constants, K_1 and K_2, are assumed to be equal to the microscopic and site-specific binding constants, k_{III} and $k_{IV,III}$ (Linse et al., 1991).

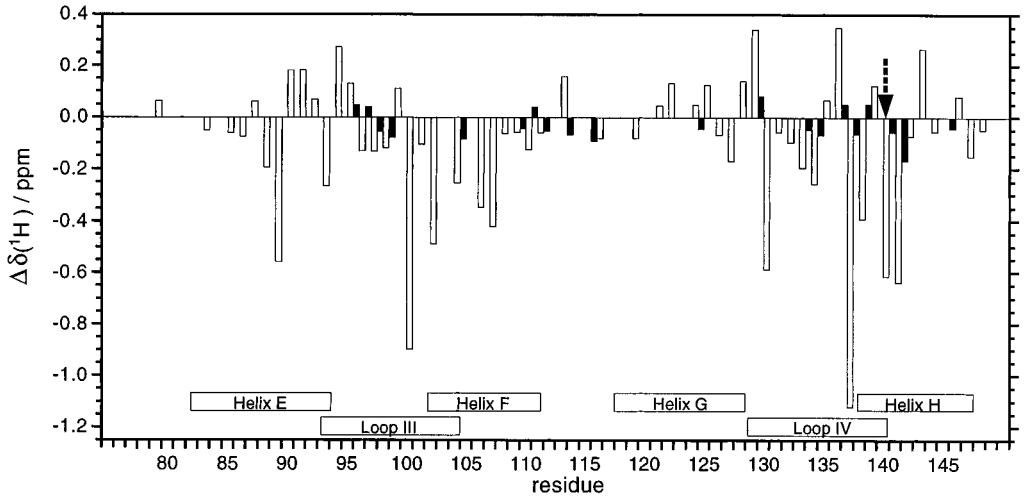

FIGURE 3: Chemical shift differences for amide protons between wt TR_2C and E140Q TR_2C at 301 K and pH 6.0. Filled and open bars correspond to the shift differences for the apo and $(Ca^{2+})_2$ states, respectively. The arrow indicates the mutation site. The location of the helices and Ca^{2+}-binding loops are indicated at the bottom.

high similarity between the two apo proteins, and the only chemical shift difference larger than 0.1 ppm is observed for the amide proton of V142, close to the mutation site. Although it is difficult to interpret chemical shift differences in terms of changes in structure and dynamics, these results indicate that the mutation causes very minute perturbations of the apo state.

$(Ca^{2+})_2$ E140Q. A comparison of the chemical shifts of the backbone amide protons between the $(Ca^{2+})_2$ states of E140Q and wt-TR_2C is shown in Figure 3 (open bars). The data of the mutant were taken on a sample with a large excess of Ca^{2+} (Ca^{2+}/protein molecular ratio 21:1) where the binding constants indicate that 97% of the protein is in the $(Ca^{2+})_2$ form (cf. below). In contrast to apo E140Q, many chemical shifts are quite different for the two $(Ca^{2+})_2$ forms, and these effects are seen in both EF hands. The largest chemical shift differences are observed for residues in helices E, F, and H, the first residues of loop IV, and for the β-sheet. The upfield chemical shift changes for a number of residues in $(Ca^{2+})_2$ E140Q are possible indications of absent or weakened hydrogen bonds. These results indicate that the mutation causes large effects on the $(Ca^{2+})_2$ state. A similar finding has been reported for the corresponding (E → Q) mutant of calbindin D_{9k}, where the $(Ca^{2+})_2$ state was found to be different from the wild-type protein as indicated by substantially different chemical shifts for many residues (Carlström & Chazin, 1993).

Several peaks are broadened in the NMR spectra of the sample with 21 equiv of calcium. However, only one set of chemical shifts is observed. The broadened peaks come from buried residues, often located in the hydrophobic core, for example, A88−K94, E104, L105, I125, Y138, and Q140−V142. It was important to check if the broadening is a consequence of the Ca^{2+}-exchange process. Using the known concentrations of Ca^{2+} and protein and the determined Ca^{2+}-binding constants, the relative populations (p_i) of the $(Ca^{2+})_1$ and the $(Ca^{2+})_2$ states were found to be 3% and 97%, respectively. As mentioned above, the E140Q mutation causes effects on the off-rate rather than the on-rate for *Drosophila* CaM (Martin et al., 1992). An off-rate of 7×10^4 s^{-1} could be calculated, using our determined binding constants of E140Q and assuming the same on-rate as for wt-TR_2C of $\sim 10^8$ s^{-1} M^{-1} (Martin et al., 1985). The contribution to the line width ($\Delta\nu_{1/2}$) from the Ca^{2+} exchange can be calculated as

$$\Delta\nu_{1/2} = \frac{4\pi(p_{Ca1})^2 p_{Ca2}\delta\nu^2}{k_{off}} \qquad (2)$$

where $\delta\nu$ is the chemical shift difference in hertz between the $(Ca^{2+})_1$ and the $(Ca^{2+})_2$ state. Assuming that the maximum chemical shift difference is ~2 ppm, as for the apo and $(Ca^{2+})_2$ states of wt-TR_2C, the line width contribution would only be 0.23 Hz, which not is consistent with broadening observed in the spectra. Furthermore, several of the nuclei, which experience large chemical shift changes upon Ca^{2+} binding, do not show broadened peaks at 21 equiv of calcium. These results indicate that the line broadening cannot be associated with the conformational changes caused by Ca^{2+} exchange.

The NOESY spectra were examined to obtain structural information about $(Ca^{2+})_2$ E140Q. The intraresidue, sequential, and medium-range NOEs were used to confirm that the secondary structure is the same as that of wt-TR_2C. When the long-range NOEs were examined in order to characterize the tertiary structure of $(Ca^{2+})_2$ E140Q, two distinct patterns of NOE cross-peaks were found. Several long-range NOEs were consistent only with either the closed apo structure or the open $(Ca^{2+})_2$ structure of wt-TR_2C. The NOEs supporting only a closed conformation are seen between protons which are 2−5 Å apart in the apo structure and 6−14 Å in the Ca^{2+}-saturated structure of wt-TR_2C. The other set of NOEs is observed for protons which are 2−5 Å apart in the Ca^{2+}-saturated structure and 6−12 Å in the apo structure. The unambiguously assigned NOEs are found in many parts of the hydrophobic core and have comparable intensities. Figure 4 shows representative NOEs from each set overlaid on NMR structures of apo (Kuboniwa et al., 1995) and $(Ca^{2+})_2$ forms (Finn et al., 1995) of the C-terminal domain of wt-CaM, illustrating the incompatibility of the two sets. Similar intensities throughout the two sets would hardly be expected if they originate from the $(Ca^{2+})_1$ and $(Ca^{2+})_2$ states since the $(Ca^{2+})_1$ state under our experimental conditions is populated to only 3%. The strong distance dependence for NOE intensities normally prevents the observation of cross-

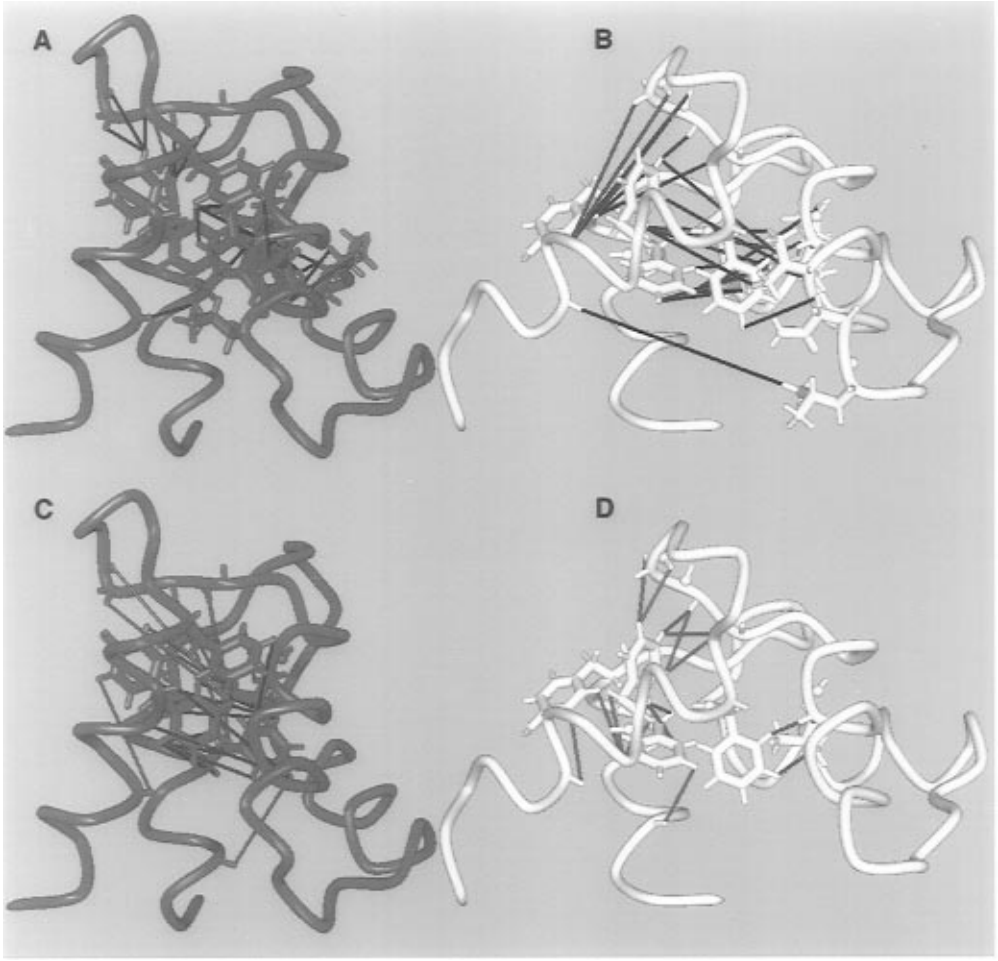

FIGURE 4: NOEs observed for $(Ca^{2+})_2$ E140Q at 301 K and pH 6.0 displayed on the solution structures of apo (A and C) and $(Ca^{2+})_2$ forms (B and D) of the C-terminal domain of wild-type calmodulin (Finn et al., 1995; Kuboniwa et al., 1995). The structure of the whole apo-CaM is used, instead of apo-TR_2C, as the side chains are more well-defined thanks to the use of multidimensional NMR techniques. (A) and (B) show NOEs in blue consistent with a closed apo-like conformation, and (C) and (D) show NOEs in red consistent with an open $(Ca^{2+})_2$-like conformation. The figure was generated using UCSF software MidasPlus (Ferrin et al., 1988).

peaks between protons at distances >5 Å (Noggle & Schirmer, 1971). For two equally populated conformations, the requirement that one conformation contributes with more than 90% to the intensity of a NOESY cross-peak is that the interproton distance in the other conformation is at least 1.44 longer. This requirement is well fulfilled for all NOEs presented in Figure 4. Thus, these mutually exclusive NOEs indicate two populated distinct conformations in $(Ca^{2+})_2$ E140Q, which appear to be similar to the open and closed structures of wt-TR_2C.

Many of the NOEs involve side chains of the aromatic residues: F89 and F92 of helix E in the N-terminal EF hand and Y138 and F141 of helix H in the C-terminal EF hand (Figure 5). Expected cross-peaks of F141 for both the closed apo and open $(Ca^{2+})_2$ structures of wt-TR_2C are seen in the NOESY spectra of $(Ca^{2+})_2$ E140Q (Figure 4). Similar parallel sets of NOE cross-peaks are found for F89, F92, and Y138. These aromatic side chains form a stabilizing aromatic cluster in the hydrophobic core in the $(Ca^{2+})_2$ state of wt-TR_2C. This aromatic cluster is not present in the apo state of wt-TR_2C where, for example, the side chain of F141 instead interacts with hydrophobic side chains from helices F and G. Upon Ca^{2+} binding to wt-TR_2C, these aromatic side chains undergo substantial movements to form the cluster.

The mutated residue 140 is situated between two of these residues, Y138 and F141 (Figure 5). In the Ca^{2+}-bound state of wt-CaM, the two side chain oxygens of E140 form two loop-stabilizing hydrogen bonds to the backbone amide protons of I130 and N137 (Strynadka & James, 1989). The E140Q mutation prevents these two hydrogen bonds from forming at the same time, and a destabilization of loop IV is expected in the Ca^{2+}-saturated state. In $(Ca^{2+})_2$ E140Q, the NOE data show that the side chain of Q140 is in close proximity to both the side chain of I130 and the backbone amide proton of N137, but at the present it cannot be determined conclusively whether both hydrogen bonds are partially populated or one is unpopulated. One possibility may be alternate hydrogen bonding in E140Q, where the closed conformation has a hydrogen bond from Q140 to N137. In the open conformation, the side chain carboxylate oxygen of Q140 has moved to establish a hydrogen bond to I130, which may be associated with the movement of F141 and the formation of the aromatic cluster in the open conformation. This mechanism would be consistent with the results of recent NMR studies of a mutated N-terminal fragment of smooth muscle TnC, where E41 in position 12 in loop I was changed to an alanine (Gagné et al., 1996; Li et al., 1996). No hydrogen bonds can be formed from the side chain of A41, and the Ca^{2+}-bound state was found to be closed. In the case of TR_2C, the formation of the aromatic

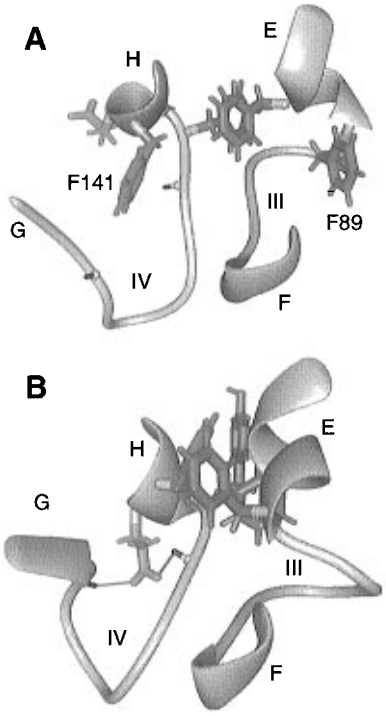

FIGURE 5: Schematic representation of the central part around the two Ca^{2+}-binding loops of the C-terminal domain of wild-type calmodulin, showing the positions of some important residues in the apo (A) and $(Ca^{2+})_2$ forms (B) (Finn et al., 1995; Kuboniwa et al., 1995). F89, F92, Y138, and F141 are displayed in red, and these four residues form an aromatic cluster in $(Ca^{2+})_2$ TR_2C. The side chain of E140, displayed in green, is pointing toward the solvent in the apo state but forms two loop-stabilizing hydrogen bonds to the backbone amide protons of I130 and N137 in the $(Ca^{2+})_2$ state. These hydrogen bonds are indicated as blue lines. The figure was generated using UCSF software MidasPlus (Ferrin et al., 1988).

cluster may provide an important driving force in order to expose the hydrophobic surface upon Ca^{2+} binding, but it does not appear to be sufficient. One additional hydrogen bond (~12 kJ/mol) may be required to shift the equilibrium toward a preponderance of the open conformation.

Typical NOE cross-peaks for both of these conformations are also found between nuclei in nonaromatic residues. Furthermore, the C-terminus of helix E has been shown to go from 3_{10} to α-helical conformation in the C-terminal domain of wt-CaM upon Ca^{2+} binding (Finn et al., 1995; Kuboniwa et al., 1995). For $(Ca^{2+})_2$ E140Q, the cross-peaks from residues in this region are broadened in the NMR spectra, indicating an exchange process.

Taking all these results together, we conclude that there is a global conformational exchange of $(Ca^{2+})_2$ E140Q between a closed apo-like conformation and an open conformation similar to the structure of the $(Ca^{2+})_2$ state of wt-TR_2C. It is important to emphasize that the chemical shifts of $(Ca^{2+})_2$ E140Q are population-weighted averages of the chemical shifts in the two different conformations according to this interpretation. This offers also a possible explanation for the observed, rather large differences in chemical shifts between the Ca^{2+}-saturated states of E140Q and wild type. Therefore, the observed upfield chemical shift changes of many amide protons in $(Ca^{2+})_2$ E140Q can be a consequence of the conformational exchange rather than a weakening of the hydrogen bonds in the open state.

An estimation of the relative population of the open and closed conformations is difficult, since even if the closed $(Ca^{2+})_2$ conformation is similar to the apo state, many chemical shifts are probably different due to the two bound calcium ions. Using the assumption that the chemical shifts of nuclei distant from the Ca^{2+}-binding loops are population-weighted averages of the chemical shifts in the apo and the $(Ca^{2+})_2$ states of wt-TR_2C, we find a population of 65 ± 15% of the open conformation in $(Ca^{2+})_2$ E140Q. Similarly, an estimation of the exchange rate is made. Using the estimated populations, the observed line broadening of resonances and the chemical shift differences between the two states of the wild-type protein give an exchange rate of $(1-7) \times 10^4$ s^{-1}. Slow motions on microsecond to millisecond time scales have earlier been found in proteins, for example, large-scale motions in the C-terminal domain of apo CaM (Tjandra et al., 1995) and in BPTI (Szyperski et al., 1993) studied by NMR using $T_{1\rho}$ experiments (Peng et al., 1991; Akke & Palmer, 1996).

Ca^{2+} Titration of E140Q. Ca^{2+}-binding curves were obtained for E140Q using 2D ^{15}N HSQC spectroscopy. The greater resolution and higher dimensionality of 2D spectroscopy offer two main advantages over 1D spectroscopy. First, the titration of a larger number of resonances can be followed, yielding greater accuracy and precision of the determined binding constants. Second, the effects of ligand binding can be directly mapped onto the amino acid sequence, thereby providing structural information. The experimental time for data collection is approximately the same for a 2D HSQC of ^{15}N-labeled material as for a standard proton 1D spectrum.

The ^{15}N HSQC spectra were well resolved and showed that the NMR spectral changes upon Ca^{2+} binding occurred in the fast to intermediate exchange regime on the NMR time scale, depending on the size of Ca^{2+}-induced chemical shift changes. The chemical shifts were plotted as a function of total Ca^{2+} concentration. For 16 amide nitrogen−proton pairs, peaks were broadened beyond detection for some intermediate Ca^{2+} concentrations, presumably due to Ca^{2+} exchange. In addition, several peaks are further broadened—a finding that we attribute to the global exchange in the Ca^{2+}-saturated state. Generally, the Ca^{2+}-binding curves exhibit biphasic profiles due to the two binding events. Neglecting effects from the gradually increased ionic strength during the titration, the observed shift under fast-exchange conditions is given as

$$\delta_{obs} = (1 - p_{Ca1} - p_{Ca2})\delta_{apo} + p_{Ca1}\delta_{Ca1} + p_{Ca2}\delta_{Ca2} \quad (3)$$

where p_{Ca1} and p_{Ca2} are the relative populations of the $(Ca^{2+})_1$ and $(Ca^{2+})_2$ forms at a given Ca^{2+} concentration. δ_{apo}, δ_{Ca1}, and δ_{Ca2} are the chemical shifts of the respective states of the protein. The population ratio of the closed and open conformations of the $(Ca^{2+})_2$ state is assumed to be constant and independent of the Ca^{2+} concentration. From the detailed Ca^{2+} titration, information could be obtained about the Ca^{2+} affinity of the two loops, the $(Ca^{2+})_1$ state, and the roles of the secondary structural elements in the two sequential binding events.

To facilitate a comparison, all curves were normalized using the initial and final chemical shift values. Figure 6A shows examples of such normalized curves. Some nuclei experience shift changes of opposite signs in each of the

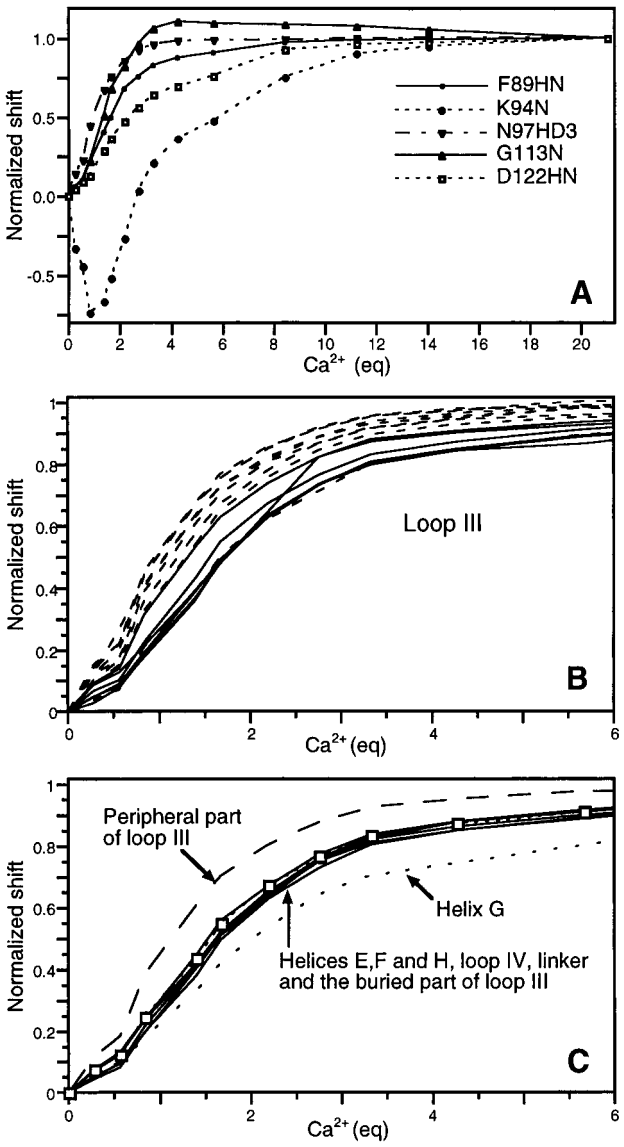

FIGURE 6: Ca^{2+}-titration curves of amide nuclei of E140Q at 301 K and pH 6.0. Each curve is normalized according to $(\delta_{obs} - \delta_{initial})/(\delta_{final} - \delta_{initial})$. Panel A shows examples of biphasic curve shapes of different amide nuclei. (The side chain amide proton, N97HD3, is located very close to the third Ca^{2+}-ligating oxygen in loop III and is consequently the nucleus most affected by the first Ca^{2+}-binding event.) The various nuclei of loop III are displayed in panel B; dashed lines correspond to peripheral residues (D95−G98) and solid lines to the other residues (D93−K94 and Y99−E104). Panel C shows the averages over the different structural elements and over the backbone nuclei in hydrophobic residues (open squares).

two Ca^{2+}-binding events, which strikingly illustrate sequential binding. The minor second apparent inflection point at approximately 6 equiv of calcium is probably due to imprecision of added calcium rather than a triphasic behavior upon Ca^{2+} binding.

Calcium Binding Constants. Wt-TR_2C binds two calcium ions with strong cooperativity with the macroscopic binding constants; $\log(K_1) = 6.45$ and $\log(K_2) = 7.45$ at low ionic strength conditions and a protein concentration of 20 μM, determined by using a competitive Ca^{2+}-binding chelator (5,5′-Br_2-BAPTA) and monitoring by UV spectroscopy (Linse et al., 1991, 1993). Using the same method, we tried to determine the binding constant of loop III,[2] but the loop binds too weakly to give an accurate value. An upper bound of $\log(K_1) = 5.2$ could be estimated, which suggests that the affinity of loop III is affected by the mutation in the other binding loop.

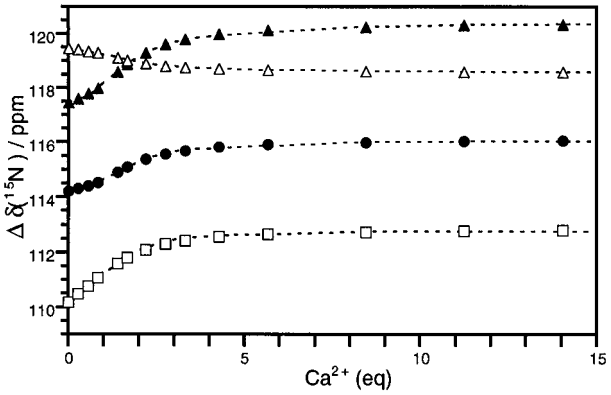

FIGURE 7: Examples of agreement of experimental (symbols) and calculated binding curves (lines) for amide nitrogens of F89 (filled circles), G98 (open squares), S101 (filled triangles), and L112 (open triangles). The calculated curves were derived from the determined binding constants and chemical shifts for apo, $(Ca^{2+})_1$, and $(Ca^{2+})_2$ E140Q.

Simultaneous fitting of Ca^{2+}-binding curves for 25 nuclei exhibiting fast exchange was made as described in the Experimental Procedures section. Since both $1/K_2$ and the protein concentration are in the millimolar range, $\log(K_2)$ could be well determined as 3.15 ± 0.10. K_1 is 2 orders of magnitude larger and consequently less accurately determined by the NMR titration method. The value of $\log(K_1)$ was determined to be 4.9 ± 0.3, with the upper limit provided by the UV experiments. The relatively small difference between K_1 and K_2 makes it impossible to obtain a sample of only the $(Ca^{2+})_1$ state. The highest possible relative population of $(Ca^{2+})_1$ E140Q is about 80% at 1.08 equiv of calcium. The final titration point with 21 equiv of calcium corresponds to 97% $(Ca^{2+})_2$ E140Q and 3% $(Ca^{2+})_1$ E140Q.

Curve Shapes and Structural Elements. Each Ca^{2+}-binding event causes chemical shift effects throughout the protein, with the major effects observed upon binding of the second calcium ion. Looking at the curve shapes in relation to the amino acid sequence, we found, as expected, that the first calcium ion binds to loop III and the second to the mutated loop IV. For example, the largest chemical shift change upon binding of the first calcium ion is observed for the side chain amide nuclei of N97 in loop III (Figure 6A). N97 is the third Ca^{2+} ligand in loop III and coordinates with the side chain oxygen.

A careful analysis reveals a heterogeneous ensemble of binding curves where the individual shapes depend on the locations of the nuclei in the protein. Individual Ca^{2+}-binding curves of amide nuclei in the N-terminus, the four helices, the linker, and the two binding loops were compared to the average curve for each structural element. The average binding curves were also compared. To avoid misinterpretations due to, for example, ionic strength effects and experimental uncertainties, we only examined binding curves for which the absolute chemical shift change from the apo to the $(Ca^{2+})_2$ state exceeded 0.1 ppm for ^1H nuclei and 0.3 ppm for ^{15}N nuclei. Two parts of the protein, the flexible N-terminus and helix G, show only small shift changes upon Ca^{2+} binding, and consequently fewer binding curves from these structural elements were compared.

The Ca^{2+}-binding curves for nuclei in the well-defined part of helix E, I85−F92, have very similar shapes. Nuclei

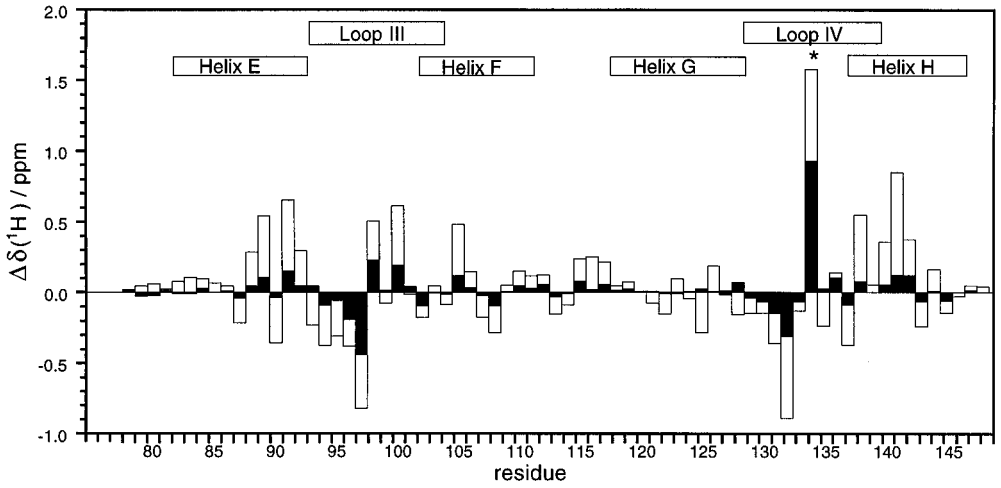

FIGURE 8: Chemical shift differences for amide protons between apo, $(Ca^{2+})_1$, and $(Ca^{2+})_2$ states of TR_2C at 301 K and pH 6.0. Filled bars show the shift differences $(Ca^{2+})_1$ E140Q − apo E140Q, and open bars show the shift differences $(Ca^{2+})_2$ wt-TR_2C − $(Ca^{2+})_1$ E140Q. The location of the helices and Ca^{2+}-binding loops are indicated at the top, and the location of G134 is indicated by a star.

within helices F and H and loop IV also respond quite similarly. The greatest variation of curve shapes is found in the linker and helix G. In helix G, a notable difference can be seen for nuclei just preceding loop IV and the other nuclei; e.g., A128 acts more as a loop IV nucleus (data not shown). A unique feature is found in the nonmutated loop III, where the nuclei can be divided into two distinct categories (Figure 6B). The behavior of the nuclei in peripheral residues (D95−G98) pointing out toward the solvent stands out from that of the other loop residues—a larger chemical shift response upon binding of the first calcium ion is observed for the peripheral nuclei. A similar observation is not made for loop IV.

Figure 6C shows average binding curves for the different structural elements. Two elements are significantly different from the others. The largest relative chemical shift response upon the first Ca^{2+} binding is observed for the peripheral part of loop III, while helix G experiences a more marked effect from the second Ca^{2+}-binding event. The other structural elements and the backbone nuclei of the hydrophobic core residues show very similar behavior. This is an intriguing observation since it indicates that loop IV is equally affected as the buried part of loop III and the hydrophobic core by the first binding event in loop III (Figure 6C). An explanation for the different shapes is found by examining the amino acid sequence and the reported three-dimensional structures of TR_2C. As expected, the binding of the first calcium ion causes chemical shift effects on the N-terminal EF-hand residues and on the linker, which, particularly in the apo state, interacts with helices E and F. Since helices E, F, and H contain most of the residues forming the hydrophobic core, the changes in helices E and F are translated to helix H. The observed chemical shift effects in loop IV may be a consequence of interactions mediated both directly by the β-sheet and/or through the hydrophobic core. The rather small magnitudes of the chemical shift changes upon binding of the first calcium ion, relative wt-TR2C, indicate that the protein is still in a predominantly closed conformation (*vide infra*).

The second Ca^{2+}-binding event causes further large effects in loop IV and also in the two surrounding helices, G and H. If as we believe a conformational exchange occurs, the C-terminal EF hand opens up part of the time, and at the same time F141 moves into the interface of helices E and H and loses its contacts with helix G. Observed effects in the N-terminal EF hand from binding of the second calcium ion are mediated by the same mechanisms as described for the binding of the first ion. Thus, the residues in loop III located in, or hydrogen-bonded to, the helices or the β-sheet are more affected than the peripheral residues pointing out toward the solvent. One of the possible signaling pathways through the β-sheet is lost due to the mutation, i.e., the interaction between the N137 in β-sheet and I130 via the hydrogen bonds formed by E140 in $(Ca^{2+})_2$ wt-TR_2C.

$(Ca^{2+})_1$ E140Q. Further insight into the structural and dynamical changes from each Ca^{2+}-binding event could be provided by the chemical shifts of the $(Ca^{2+})_1$ state. The chemical shifts of the $(Ca^{2+})_1$ state cannot be obtained directly from the NMR spectra, as this state is never populated to more than about 80%, but were obtained from an individual fit of eq 3 to each Ca^{2+}-binding curve. The populations of the apo, $(Ca^{2+})_1$, and $(Ca^{2+})_2$ forms were calculated for each titration point from the binding constants and the known concentrations of Ca^{2+} and protein. This approach must, however, be considered as an approximation for residues having broadened resonances due to Ca^{2+} exchange, since the chemical shift for nuclei in intermediate exchange between unequally populated states also will depend on the kinetics (Sandström, 1982). A comparison of the calculated binding curves and the experimentally determined curves shows in most cases excellent agreement. A selection of fitted curves are presented in Figure 7. Less good agreement was, however, found for a few residues. These include the residues in the beginning of the N-terminus (data not shown). One explanation might be that effects on the chemical shift due to the increased ionic strength during the Ca^{2+} titration are comparable to the small total chemical shift changes induced by binding of the two calcium ions.

A graphical comparison of the amide proton chemical shifts of the apo, $(Ca^{2+})_1$, and $(Ca^{2+})_2$ states of TR_2C is shown in Figure 8. Since $(Ca^{2+})_2$ E140Q is subject to global conformational exchange, we have chosen to use $(Ca^{2+})_2$ wt-TR_2C as our reference for the chemical shifts of a "true" open state of the TR_2C domain. Filled bars correspond to shift changes induced by binding of the first calcium ion and open bars to binding of the second ion. Positive and

negative values correspond to downfield and upfield shift changes, respectively. Generally, only small relative shift changes are observed upon binding of the first calcium ion to loop III in the mutant. This indicates that only minor conformational changes occur and, therefore, that the $(Ca^{2+})_1$ state appears to be similar to the closed apo structure. This supports earlier studies of *Drosophila* CaM, which indicate that the E140Q mutant with only one bound calcium ion to the C-terminal domain has not adopted the structure of $(Ca^{2+})_2$ wt-TR_2C (Maune et al., 1992a; Gao et al., 1993). Whether or not $(Ca^{2+})_1$ E140Q experiences exchange between two or more conformations cannot be determined from these data, since NOESY spectra of the pure $(Ca^{2+})_1$ state of E140Q cannot be recorded. If such an exchange exists, the position of the equilibrium must, however, be shifted toward a closed conformation as indicated by the rather close similarity between the chemical shifts of the apo and $(Ca^{2+})_1$ states.

A proposed mechanism for the cooperative Ca^{2+} binding in domains of the nonregulatory EF-hand proteins, like calbindin D_{9k}, is that the first calcium ion causes most of the substantial structural and dynamical changes on the route to the final $(Ca^{2+})_2$ state and thus facilitates binding of the second ion to a somewhat preformed loop (Akke et al., 1991). The finding of an essentially closed conformation of $(Ca^{2+})_1$ E140Q suggests that this model may not be strictly applicable for regulatory EF-hand proteins. Our results have at least three possible explanations: (1) Ca^{2+} binding to the C-terminal EF-hand is needed for the protein to change to an open conformation, (2) Ca^{2+} binding to both EF hands is needed for the conformational change to occur, or (3) E140 is essential for the opening when Ca^{2+} binds in loop III.

It may, of course, be that $(Ca^{2+})_1$ E140Q is not an ideal model for studies of the $(Ca^{2+})_1$ intermediate of the wild-type protein. It appears, however, that some features of the intramolecular signaling mechanism in E140Q are also applicable for wt-CaM. For example, in addition to the expected chemical shift effects in Ca^{2+}-binding loop III in $(Ca^{2+})_1$ E140Q, large shift changes are observed in the empty loop IV. In particular, residues D131, G132, and G134 in the beginning of the loop experience substantial chemical shifts changes toward those of $(Ca^{2+})_2$ wt-TR_2C (Figure 8). The increase in amide proton shift of G134 implies that the hydrogen bond to one of the side chain carboxylate oxygens in D129 is strengthened. This carboxylate group provides a center around which the first six residues in the loop fold when the calcium ion is bound (Strynadka & James, 1989). This suggests some rearrangement of the empty loop IV toward the conformation taken up in the Ca^{2+}-bound form and consequently an increased affinity for the second calcium ion. The interaction between loop III and loop IV may be mediated either through the hydrophobic core and/or by the β-sheet between the two loops. A similar rearrangement might occur in the wild-type protein and, hence, contribute to the cooperativity.

In addition to the above discussions, a passive role of helix G during the Ca^{2+}-binding event in the N-terminal EF-hand is indicated by the close similarity between the chemical shifts of this helix in the apo and $(Ca^{2+})_1$ states. As stated earlier, helix G is less tightly packed to the hydrophobic core and is consequently less affected by Ca^{2+} binding to the N-terminal EF hand. It is interesting to note that certain residues in the β-sheet and in helices F and G experience chemical shift changes in the opposite direction as compared to wt-TR_2C. This suggests local conformational changes of these residues, which do not take place in wt-TR_2C.

CONCLUDING REMARKS

The present study of E140Q shows that mutation of the glutamic acid in the 12th position of binding loop IV has large effects on the $(Ca^{2+})_2$ state and on both Ca^{2+}-binding loops. NOESY data indicate that the $(Ca^{2+})_2$ state experiences exchange between two conformations which appear to be similar to the closed apo and open $(Ca^{2+})_2$ structures observed in wt-TR_2C. A hypothesis is that the conformational exchange is associated with the inability of the side chain of Q140 to form the two simultaneous hydrogen bonds to the backbone amide protons of I130 and N137 occurring in $(Ca^{2+})_2$ wt-TR_2C.

Each Ca^{2+}-binding event to E140Q causes substantial chemical shift effects on the backbone nuclei of the whole protein. Exceptions are the N-terminus and helix G, which are mainly affected by the binding of the second calcium ion to loop IV. The conformation of the $(Ca^{2+})_1$ state appears to be essentially closed, and the major structural changes are observed upon binding of the second calcium ion. The E140Q mutation, however, prevents the protein from completely exposing the hydrophobic surface and fully adopting the wild-type $(Ca^{2+})_2$ structure. Again, the formation of the two hydrogen bonds from the side chain of E140 might be a crucial key for the structural change to occur upon Ca^{2+} binding, which earlier has been proposed for calbindin D_{9k} by Wimberly et al. (1995). This study has emphasized the critical importance of E140 in wt-CaM and that the site-specific mutation has far-reaching effects on the structure of TR_2C.

This characterization of the E140Q mutant has provided valuable information regarding the mechanism for the Ca^{2+} binding in native CaM. Our results may shed light on earlier studies of CaM, using equivalent mutants. The dynamic interchange of two substantially different conformations inferred for $(Ca^{2+})_2$ E140Q is currently the subject of further investigations. In addition, other mutants need to be studied in detail, for better characterization of the wild-type intermediates of TR_2C and CaM in the Ca^{2+}-binding processes. The ideal properties of such a mutant would be that the structures of the apo and the $(Ca^{2+})_2$ states are similar to those of wt-CaM but that pure sequential binding is obtained.

ACKNOWLEDGMENT

We thank Drs. Mikael Akke, Bryan Finn, Sara Linse, and Torbjörn Drakenberg for helpful comments and stimulating discussions. Dr. Per-Åke Malmquist was helpful in providing a suitable algorithm for the determination of binding constants.

SUPPORTING INFORMATION AVAILABLE

One table of the backbone $^1H-$ and $^{15}N-$amide assignments of apo, $(Ca^{2+})_1$, and $(Ca^{2+})_2$ states of E140Q (2 pages). Ordering information is given on any current masthead page.

REFERENCES

Akke, M., & Palmer, A. G., III (1996) *J. Am. Chem. Soc. 118*, 911−912.

Akke, M., Forsén, S., & Chazin, W. J. (1991) *J. Mol. Biol. 220*, 173−189.
Aue, W. P., Batholdi, E., & Ernst, R. R. (1976) *J. Chem. Phys. 64*, 2229−2246.
Babu, Y. S., Bugg, C. E., & Cook, W. J. (1988) *J. Mol. Biol. 204*, 191−204.
Barbato, G., Ikura, M., Kay, L. E., Pastor, R. W., & Bax, A. (1992) *Biochemistry 31*, 5269−5278.
Bax, A. (1985) *J. Magn. Reson. 65*, 142−145.
Beckingham, K. (1991) *J. Biol. Chem. 266*, 6027−6030.
Brodin, P., Grundström, T., Hofmann, T., Drakenberg, T., Thulin, E., & Forsén, S. (1986) *Biochemistry 25*, 5371−5377.
Carlström, G., & Chazin, W. J. (1993) *J. Mol. Biol. 231*, 415−430.
Cavanagh, J., & Rance, M. (1992) *J. Magn. Reson. 96*, 670.
Chattopadhyaya, R., Meador, W. E., Means, A. R., & Quiocho, F. A. (1992) *J. Mol. Biol. 228*, 1177−1192.
Chazin, W. J., & Wright, P. E. (1987) *Biopolymers 26*, 973−977.
Crivici, A., & Ikura, M. (1995) *Annu. Rev. Biophys. Biomol. Struct. 24*, 85−116.
Drabikowski, W., Kuznicki, J., & Grabarek, Z. (1977) *Biochim. Biophys. Acta 485*, 124−133.
Ferrin, T. E., Huang, C. C., Jarvis, L. E., & Langridge, R. (1988) *J. Mol. Graphics 6*, 13−27.
Finn, B. E., & Forsén, S. (1995) *Structure 3*, 7−11.
Finn, B. E., Drakenberg, T., & Forsén, S. (1993) *FEBS Lett. 336*, 368−374.
Finn, B. E., Evenäs, J., Drakenberg, T., Waltho, J. P., Thulin, E., & Forsén, S. (1995) *Nat. Struct. Biol. 2*, 777−783.
Gagné, S. M., Tsuda, S., Li, M. X., Smillie, L. B., & Sykes, B. D. (1995) *Nat. Struct. Biol. 2*, 784−789.
Gagné, S. M., Li, X. S., & Sykes, B. D. (1996) *Science* (submitted for publication).
Gao, Z. H., Krebs, J., VanBerkum, M. F., Tang, W. J., Maune, J. F., Means, A. R., Stull, J. T., & Beckingham, K. (1993) *J. Biol. Chem. 268*, 20096−20104.
George, S. E., Su, Z., Fan, D., Wang, S., & Johnson, D. J. (1996) *Biochemistry 35*, 8307−8313.
Hartel, A. J., Lankhorst, P. P., & Altona, C. (1982) *Eur. J. Biochem. 129*, 343−357.
Herzberg, O., & James, M. N. G. (1988) *J. Mol. Biol. 203*, 761−779.
Klee, C. B. (1988) in *Molecular Aspects of Cellular Regulation* (Cohen, P., & Klee, C. B., Eds.) pp 35−56, Elsevier, New York.
Kretsinger, R. H., & Nockolds, C. E. (1973) *J. Biol. Chem. 248*, 3313−3326.
Kördel, J., Skelton, N. J., Akke, M., & Chazin, W. J. (1993) *J. Mol. Biol. 231*, 711−734.
Kuboniwa, H., Tjandra, N., Grzesiek, S., Ren, H., Klee, C. B., & Bax, A. (1995) *Nat. Struct. Biol. 2*, 768−776.
Li, X. S., Gagné, S. M., Kloks, C., Chandra, M., Audette, G., Smillie, L. B., & Sykes, B. D. (1996) *Biochemistry* (submitted for publication).
Linse, S., Helmersson, A., & Forsén, S. (1991) *J. Biol. Chem. 266*, 8050−8054.
Linse, S., Thulin, E., & Sellers, P. (1993) *Protein Sci. 2*, 985−1000.
Macura, S., & Ernst, R. R. (1980) *Mol. Phys. 41*, 95−117.
Martin, S. R., Andersson Teleman, A., Bayley, P. M., Drakenberg, T., & Forsén, S. (1985) *Eur. J. Biochem. 151*, 543−550.
Martin, S. R., Maune, J. F., Beckingham, K., & Bayley, P. M. (1992) *Eur. J. Biochem. 205*, 1107−1114.
Maune, J. F., Beckingham, K., Martin, S. R., & Bayley, P. M. (1992a) *Biochemistry 31*, 7779−86.
Maune, J. F., Klee, C. B., & Beckingham, K. (1992b) *J. Biol. Chem. 267*, 5286−5295.
Noggle, J. H., & Schirmer, R. E. (1971) *The Nuclear Overhauser Effect: Chemical Applications*, Academic Press, New York.
Orbons, L. P. M., van der Marel, G. A., van Boom, J. H., & Altona, C. (1987) *Eur. J. Biochem. 170*, 225−239.
Peng, J. W., Thanabal, V., & Wagner, G. (1991) *J. Magn. Reson. 94*, 82−100.
Sandström, J. (1982) *Dynamic NMR Spectroscopy*, 1 ed., Academic Press Inc., London.
Shaka, A. J., Keeler, J., Frenkiel, T., & Freeman, R. (1983) *J. Magn. Reson. 52*, 335−338.
Shea, M. A., Verhoeven, A. S., & Pedigo, S. (1996) *Biochemistry 35*, 2943−2957.
Skelton, N. J., Kördel, J., Akke, M., Forsén, S., & Chazin, W. J. (1994) *Nat. Struct. Biol. 1*, 239−245.
Starovasnik, M. A., Su, D. R., Beckingham, K., & Klevit, R. E. (1992) *Protein Sci. 1*, 245−253.
Strynadka, N. C. J., & James, M. N. G. (1989) *Annu. Rev. Biochem. 58*, 951−998.
Szebenyi, D. M. E., & Moffat, K. (1986) *J. Biol. Chem. 261*, 8761.
Szyperski, T., Luginbühl, P., Otting, G., Güntert, P., & Wütrich, K. (1993) *J. Biomol. NMR 3*, 151−164.
Thulin, E., Andersson, A., Drakenberg, T., Forsén, S., & Vogel, H. J. (1984) *Biochemistry 23*, 1862−1870.
Tjandra, N., Kuboniwa, H., Ren, H., & Bax, A. (1995) *Eur. J. Biochem. 230*, 1014−1024.
Walsh, M., Stevens, F. C., Kuznicki, J., & Drabikowski, W. (1977) *J. Biol. Chem. 252*, 7440−7443.
Wimberly, B., Thulin, E., & Chazin, W. J. (1995) *Protein Sci. 4*, 1045−1055.
Wishart, D. S., Bigam, C. G., Yao, J., Abildgaard, F., Dyson, H. J., Oldfield, E., Markley, J. L., & Sykes, B. D. (1995) *J. Biomol. NMR 6*, 135−140.
Zhang, M., Tanaka, T., & Ikura, M. (1995) *Nat. Struct. Biol. 2*, 758−767.
Zhang, O., Kay, L. E., Olivier, J. P., & Forman-Kay, J. D. (1994) *J. Biomol. NMR 4*, 845−858.

BI9628275